ELSEVIER

Journal of Membrane Science 204 (2002) 53–65

journal of MEMBRANE SCIENCE

www.elsevier.com/locate/memsci

Design parameters for rotating cylindrical filtration

John A. Schwille, Deepanjan Mitra, Richard M. Lueptow*

Department of Mechanical Engineering, Northwestern University, Evanston, IL 60208, USA

Received 20 September 2001; received in revised form 17 December 2001; accepted 4 January 2002

Abstract

Rotating cylindrical filtration displays significantly reduced plugging of filter pores and build-up of a cake layer, but the number and range of parameters that can be adjusted complicates the design of these devices. Twelve individual parameters were investigated experimentally by measuring the build-up of particles on the rotating cylindrical filter after a fixed time of operation. The build-up of particles on the filter depends on the rotational speed, the radial filtrate flow, the particle size and the gap width. Other parameters, such as suspension concentration and total flow rate are less important. Of the four mechanisms present in rotating filters to reduce pore plugging and cake build-up, axial shear, rotational shear, centrifugal sedimentation and vortical motion, the evidence suggests rotational shear is the dominant mechanism, although the other mechanisms still play minor roles. The ratio of the shear force acting parallel to the filter surface on a particle to the Stokes drag acting normal to the filter surface on the particle due to the difference between particle motion and filtrate flow can be used as a non-dimensional parameter that predicts the degree of particle build-up on the filter surface for a wide variety of filtration conditions.

Keywords: Microfiltration; Fouling; Dynamic filtration

1. Introduction

Rotating cylindrical filtration offers a means of dynamic filtration that minimizes the plugging of the filter pores with particles and the build-up of a cake layer. The essence of a rotating filter is a porous inner cylinder rotating concentrically within an outer non-porous cylinder. The suspension enters the annular gap at one end of the annulus. Filtrate passes through the inner porous cylinder and is removed through a hollow shaft. Concentrate is removed from the annular gap at the end of the device opposite the suspension entrance.

In the design and operation of a rotating filter, there are a large number of variables that affect the filtration performance including operational parameters that can be varied by the device operator, suspension parameters that are dependent on the physical characteristics of the suspension that is being filtered, and geometric parameters that are related to the physical dimensions of the device. Table 1 lists the key parameters, each of which can be expressed in terms of the dimensionless quantities listed in the far right column of the table.

Previous research into the effect of these variables has been performed for only a sparse set of configurations and parameters. Some of the earliest work in rotating filtration was reported by Hallström and Lopez-Leiva [1] for ultrafiltration of skim milk. They were able to quadruple the flux by rotating the cylindrical filter at high speeds. This increase in filtration flux based on angular velocity has also been seen by other researchers [2–6]. Initial research on the influence of

* Corresponding author. Tel.: +1-847-491-4265; fax: +1-847-491-3915.
E-mail address: r-lueptow@northwestern.edu (R.M. Lueptow).

0376-7388/02/$ – see front matter
PII: S0376-7388(02)00016-9

Nomenclature

d	annular gap width
D	diameter
F	force
h	length of inner cylinder
h_f	length of filter portion of inner cylinder
J	filtrate flux
Q	volumetric flow rate
r	radius
Re	Reynolds number (Table 1)
St	Stokes number (Eq. (4))
Ta	Taylor number (Table 1)
V	velocity
$\forall$	volume

Greek letters

ϕ	concentration
γ_w	shear rate at the wall
Γ	aspect ratio (h/d)
η	radius ratio (r_i/r_o)
μ	dynamic viscosity
ν	kinematic viscosity
ρ	density
ρ'	density difference ratio
τ_w	shear stress at the wall
Ω	angular velocity

Subscripts

a	axial
c	critical
D	drag
f	fluid
feed	suspension feed
i	inner
o	outer
p	particle
r	radial
s	solid
τ	shear
θ	tangential

the annular gap width indicated that smaller annular gaps between the cylindrical filter and the outer cylindrical shell result in higher membrane flux due to higher shear rates [7]. Suspension variables such as feed rates and concentration seem to have a minimal effect, while results for the effect of particle size are inconclusive [8,9].

Four mechanisms in rotating cylindrical filtration could be responsible for the higher flux in rotating filtration, all related to reduced plugging of the membrane pores and build-up of particles on the membrane surface: (1) the axial shear due to the annular Poiseuille flow between the two cylinders, (2) the rotational shear due to the circular Couette flow created by the high rotational speed of the inner cylinder, (3) the centrifugal sedimentation produced by the rotational field, and (4) the washing of particles away from the filter surface by a secondary vortical flow known as Taylor vortices consisting of pairs of counter-rotating toroidal vortices that fill the annular gap between differentially-rotating cylinders [10]. The critical conditions at which these vortices first appear depends on the Taylor number, or rotating Reynolds number, $Ta = \Omega r_i d/\nu$, where Ω is the angular velocity of the inner cylinder, d the gap width between the two cylinders, r_i the radius of the inner cylinder, and ν is the fluid's kinematic viscosity. The critical Taylor number above which vortices appear depends on the radius ratio, $\eta = r_i/r_o$, where r_o is the radius of the outer cylinder. At higher Taylor numbers the vortices become stronger and may develop waviness or become turbulent.

Given the large number of parameters in rotating cylindrical filtration, it is a difficult to know which combination of values for the parameters will result in optimal flux for a given situation. Thus, this experimental investigation has two major goals: (1) identify the most important parameters involved in the prevention of particles building up on the surface of a rotating cylindrical filter and quantify their effects, (2) identify which of the four mechanisms (axial shear, rotational shear, centrifugal sedimentation, or vortical motion) is responsible for the minimization of pore plugging and cake build-up (and consequently high flux) in rotating filtration. Although the focus is on the build-up of particles (a cake layer) on the surface of a rotating cylindrical filter, it is reasonable to assume that the conditions that reduce the build-up of particles would also reduce concentration polarization and minimize the plugging of membrane pores by particles in rotating cylindrical filters, thereby reducing the problem of fouling.

Table 1
Parameters in rotating cylindrical filtration

Parameter type	Parameter	Dimensionless quantity	
Operational parameters	Angular velocity (Ω)	Taylor number	$Ta = \Omega r_i d/\nu$
	Radial flow rate (Q_r)	Radial Reynolds number	$Re_r = Q_r d/2\nu\pi r_i h_f$
	Axial flow rate (Q_a)	Axial Reynolds number	$Re_a = Q_a d/\nu\pi(r_o^2 - r_i^2)$
Suspension parameters	Particle density (ρ_p)	Density difference ratio	$\rho' = (\rho_p - \rho_f)/\rho_f$
	Particle diameter (D_p)	Particle Taylor number	$[(\rho_p - \rho_f)/\rho_f][D_p^2\Omega/18\nu]$
	Suspension concentration (ϕ_{feed})		$\phi_{feed} = V_s/V_{total}$
	Fluid density (ρ_f)	Density difference ratio	$\rho' = (\rho_p - \rho_f)/\rho_f$
	Kinematic viscosity ($\nu_f = \mu_f/\rho_f$)		
Geometric parameters	Cylinder radii (r_i, r_o)	Radius ratio	$\eta = r_i/r_o$
	Gap width (d)	Gap width to particle diameter	d/D_p
	Filter height (h)	Aspect ratio	$\Gamma = h/d$
	Filter pore diameter (D_{pore})	Particle diameter to pore diameter	D_p/D_{pore}

2. Experimental methods

The test cell shown in Fig. 1 was used to examine the effect of the filtration parameters on the degree of particle build-up on the filter surface. The device consisted of an inner porous filter cylinder to separate particles from the fluid, and an outer cylinder housing. The filter medium was a porous polyethylene cylinder with a wall thickness of 4.5 mm and a pore size of 5, 10, 15, or 60 μm, according to the manufacturer. A hollow aluminum cylinder slightly smaller than the inner diameter of the filter cylinder formed a 1.9 mm annular gap just inside of the filter permitting the axial flow of the filtrate to radial channels at the right end of the rotating assembly leading to the filtrate outlet. For the majority of the experiments, the filter outer diameter was 4.95 cm. A small number of experiments were performed with filter diameters of 4.70 cm and 3.86 cm. The length of the filter surface was $h_f = 12.11$ cm, and the overall length of the filter chamber was $h = 12.74$ cm. The inner diameter of the outer cylinder was 5.30 cm. The suspension entered the horizontally oriented test cell through a radial port at the left end and top of the outer cylinder housing.

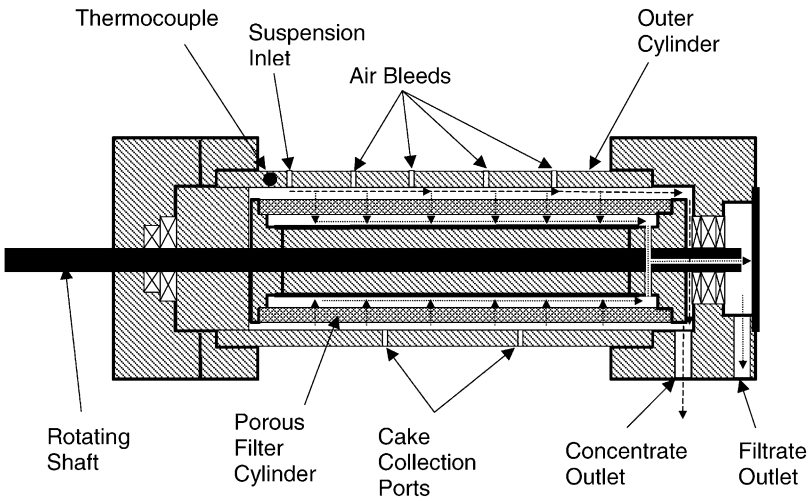

Fig. 1. Schematic of the rotating filter test cell (not to scale)

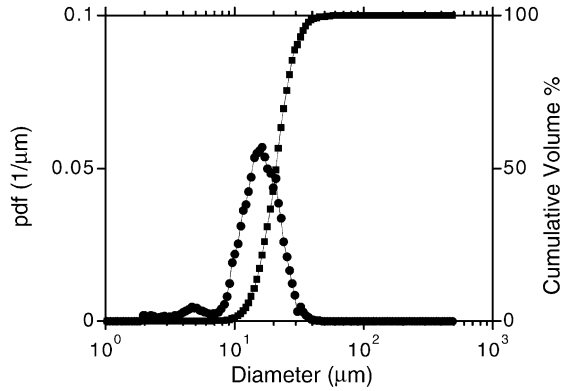

Fig. 2. Distribution of nylon particles having a volumetric median diameter of 22 μm: (●) probability density function, (■) cumulative volume percent.

The concentrate and filtrate were removed via ports in the end block assembly at the right end of the test cell. Several Air Bleed ports along the top of the cylinder housing were necessary to purge air when the system was primed. Upon reversing the filtrate flow at the end of an experiment, cake collection ports along the bottom of the outer cylinder housing permitted the removal of particles that had collected on the filter surface and in the pores of the filter. A direct-drive stepper motor and controller were used to rotate the inner cylindrical filter. Rotational speeds ranged from 0 to 500 rpm corresponding to Taylor numbers from 0 to 2200.The test suspension was typically 0.15 vol.% of nylon particles in water with a very small quantity of surfactant added to disperse the particles. The particles had a density of 1.16 g/cm^3 and a volumetric median diameter of 22 μm. A typical particle size distribution measured using a laser based optical particle counter (Particle Sizing Systems Accusizer Model 770) is shown in Fig. 2. While the particle distribution was not monodisperse, the range of particle sizes was fairly narrow. Three other particles having different densities and size distributions were also used for a small number of experiments, as described later.

After priming the test cell and flow circuit with pure water, suspension from a stirred reservoir was introduced into the test cell by a peristaltic pump. Having passed through the rotating porous filter cylinder, the filtrate flowed axially in the annulus between the outer wall of the aluminum cylinder and the inner wall of the porous filter cylinder, exiting the device via a hollow shaft. The filtrate flow rate was measured using a turbine flowmeter. The increasingly concentrated suspension flowed axially from left to right in the annulus between the rotating porous filter cylinder and the outer cylinder housing. The concentrate was pumped out of the test cell at the opposite end that the suspension entered using a second peristaltic pump, set at a lower flow rate than the inlet suspension pump. Thus, the filtrate flow rate was controlled by the difference between the inlet suspension pump flow rate and the concentrate pump flow rate. The use of peristaltic pumps introduced a slight pulsatile motion to the flow. A pulse-damping chamber proved to trap particles, so it could not be used. Careful observation of the flow and the cake layer indicated that the pulsations did not cause noticeable axial acceleration of particles in the annulus, periodic changes in the cake layer, or changes in the nature of the vortical motion.

Each experimental trial lasted for 10 min of suspension flow, after which the suspension flow was shut-off and the test cell was isolated by clamping the inlet and outlets. Depending on flow conditions, particles would build up to varying degrees on the surface of the rotating porous cylinder forming a thin “cake layer” during the experiment. These particles were back-flushed off the porous cylinder and collected via the cake collection ports at the bottom of the test cell. In order to quantify filtration performance and the prevention of particle build-up on the filter surface at the end of an experiment, typically three samples each were obtained of the inlet suspension feed, the filtrate, the concentrate, and the back-flush of the cake layer. The particle concentrations for these samples were measured using the optical particle counter. The standard deviation for the particle concentration measured for the three samples was 5% of the measured concentration on average. However, the standard deviation in a small number of cases (about 5% of the experiments) was substantially higher.

The percentage of total volume of particles entering the device that remained in the cake layer at the end of the experiment, which we call “% cake layer,” was used as a measure of the particle build-up on the filter surface for a given set of operating, geometric, and suspension parameters. A high percentage indicates substantial cake layer build-up for a given filtration configuration, while a low percentage indicates

a minimal cake layer. Inevitable in any experiment like this is the "loss" of particles for a variety of reasons. A mass balance of particles resulted in accounting for 95% on average. Particles were typically lost due to adhesion to the walls of fluid passageways.

Of course, using the approach described above permits the characterization of the cake build-up from the standpoint of a "batch unit operation." By this we mean that neither the transient build-up of the cake layer nor the details of the flows within the device were considered. For instance, because fluid was removed through the inner cylinder, the suspension became more concentrated and moved more slowly as it progressed axially in the device. This most likely resulted in somewhat different conditions at different axial locations in the device. While these details are important to the operation of a rotating cylindrical filter device, our goal of identifying the most important parameters in the effective operation of the device are well-served by the "batch unit operation" approach that we have taken.

3. Results and discussion

Overall, 97 experimental trials were conducted changing all of the 12 parameters listed in Table 1. Unless otherwise noted, the experiments were for the following conditions. The suspension was of particles having a volumetric median diameter of $D_p = 22\,\mu m$ and a density of $\rho_p = 1.16\,g/cm^3$ and deionized water ($\rho' = 0.16$) with a volume concentration of $\phi_{feed} = 0.15\%$. The filter pore size was $10\,\mu m$ ($D_p/D_{pore} = 2.2$) and the gap between the porous inner filter and the housing was 1.7 mm ($\eta = 0.935$ and $d/D_p = 77$). The inlet flow rate was about 6 ml/s ($Re_a = 37.0$), 93% of which was directed through the filter ($Re_r = 0.51$).

The effect of the rate of rotation on cake layer for a number of angular velocities and filtrate flow conditions is shown in Fig. 3. The vertical axis indicates the degree of particle build-up on the filter surface in terms of the percentage of particles that entered the rotating filter test cell that end up in the cake layer (% cake layer); the horizontal axis is the percentage of the approximately 6 ml/s flow rate entering the device that passes through the filter (corresponding to

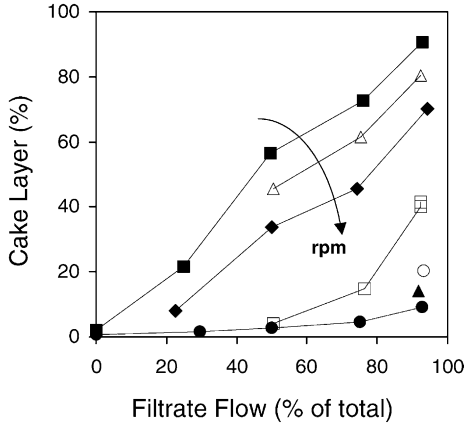

Fig. 3. The dependence of the percentage of particles in the cake layer on the filtrate flow and rotational speed: (■) 0 rpm ($Ta/Ta_c = 0$), (△) 45 rpm ($Ta/Ta_c = 1.24$), (◆) 100 rpm ($Ta/Ta_c = 2.76$), (□) 200 rpm ($Ta/Ta_c = 5.51$), (○) 300 rpm ($Ta/Ta_c = 8.27$), (▲) 400 rpm ($Ta/Ta_c = 11.02$), (●) 500 rpm ($Ta/Ta_c = 13.78$) ($D_p = 22\,\mu m$, $D_{pore} = 10\,\mu m$, $\phi_{feed} = 0.15\%$, $Q_{in} = 6$ ml/s).

$0 < Re_r < 0.55$). Zero percent flow through the filter results in no particles in the cake layer, as would be expected. Approaching 100% flow through the filter results in essentially "dead-end" filtration. Clearly, the cake layer has a strong dependence on both the filtrate flow and the rotational speed. For no rotation and a high percentage of flow through the filter, nearly 100% of the particles entering the device end up in the cake layer. However, rotation reduces the number of particles in the cake layer substantially even at very high flow rates through the filter. At the highest rotational speed, the cake layer is quite small for any filtrate flow. This demonstrates the advantage of rotating filtration in preventing the build-up of particles on the filter surface. The duplicate data points for 200 rpm at 93% filtrate flow suggest the degree of repeatability for small and moderate cake layer build-up. As will be shown later, the data was less repeatable for higher cake layer percentages (above 70%).

This data can be cross-plotted in order to emphasize other aspects of the physics underlying rotating filtration. Fig. 4 shows the dependence of the percentage of particles ending up in the cake layer on the rotational speed for approximately 93% of the inlet flow passing through the filter. Here the rotational speed is expressed as the Taylor number normalized

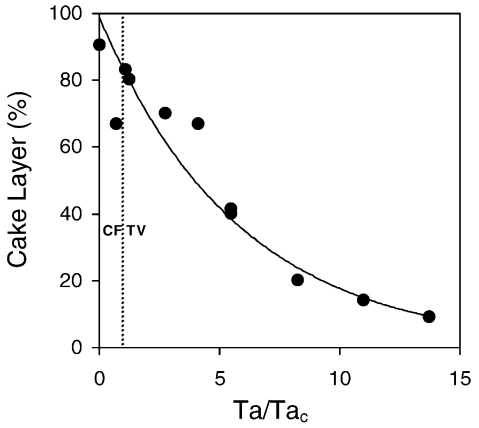

Fig. 4. The dependence of the percentage of particles in the cake layer on rotational speed at 93% inlet suspension flow through the filter. The dotted line at $Ta/Ta_c = 1$ is the transition to vortical flow at 36.3 rpm. CF indicates Couette flow (no vortices), TV indicates Taylor vortices ($D_p = 22\,\mu m$, $D_{pore} = 10\,\mu m$, $\phi_{feed} = 0.15\%$, $Q_{in} = 6$ ml/s, 93% flow through filter).

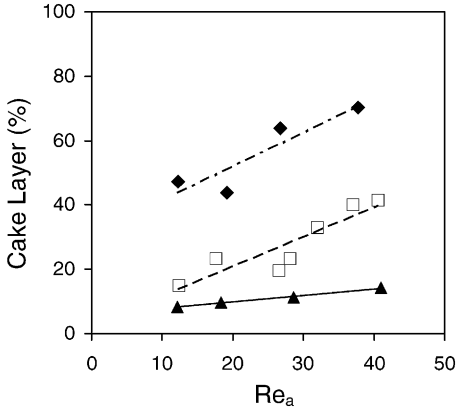

Fig. 5. Dependence of the percentage of particles in the cake layer on the inlet suspension flow rate: (◆) 100 rpm ($Ta/Ta_c = 2.76$), (□) 200 rpm ($Ta/Ta_c = 5.51$), (▲) 400 rpm ($Ta/Ta_c = 11.02$). Lines are least squares fits to the data ($D_p = 22\,\mu m$, $D_{pore} = 10\,\mu m$, $\phi_{feed} = 0.15\%$, 93% flow through filter).

by the critical Taylor number, Ta_c, necessary for vortex formation. The percentage of particles ending up in the cake layer decreases as the rotational speed increases. The solid curve is an exponential least squares fit to the data. The theoretical critical angular velocity for the appearance of Taylor vortices at $Ta/Ta_c = 1$ ($Ta_c = 162$ for this radius ratio [11]) is also shown. If the Taylor vortices were the underlying cake prevention mechanism in rotating filtration, the cake layer percentage would be expected to change dramatically as rotational speed increases from below the transition value to above the transition value. However, no sharp change is evident in Fig. 4 within experimental variability. This evidence discounts the direct importance of Taylor vortices as a significant mechanism for reducing the build-up of particles on the filter surface. However, the continuous decrease in the cake layer with increasing Ta/Ta_c suggests that rotational shear, which increases monotonically with rotational speed, is a significant factor in minimizing the build-up of particles on the filter surface in rotating filtration.

Previous researchers [2–6] have varied rotational speed and also found that increasing rotational speed increases some measure of filtration effectiveness. However, while other researchers have attributed some of the increased effectiveness to Taylor vortices, the results in Fig. 4 are the first that focus on the transition from non-vortical to vortical flow in order to clarify the vortices' role in minimizing cake layer build-up for rotating filtration.

The dependence of the cake layer on the inlet suspension flow rate is shown in Fig. 5. The inlet suspension flow rate was varied from 1.95 to 6.60 ml/s, corresponding to axial Reynolds numbers from 12.1 to 41.0 at the inlet. An increase in the inlet suspension flow results in a higher percentage of the particles remaining in the cake layer at the end of the experiment. The higher throughput also results in a greater number of particles in the cake layer, in spite of the higher axial flow that occurs in the annulus and the accompanying higher axial shear. Thus, high throughput conditions present significant challenges to a rotating filter. However, the advantages of rotation are again clearly evident. At the highest rotational speed, the cake percentage is much less than the other rotational speeds and the increase in cake percentage with increasing inlet flow rate is significantly lower at higher rates of rotation. These results are slightly different than previously seen for a suspension of silica slurry where the feed flow rate had almost no effect on the filtrate flux [8]. However, the rotational speed in those experiments was very high ($Ta = 14{,}900$), and the range of feed flow rates was not large, only 1.58–3.96 ml/s.

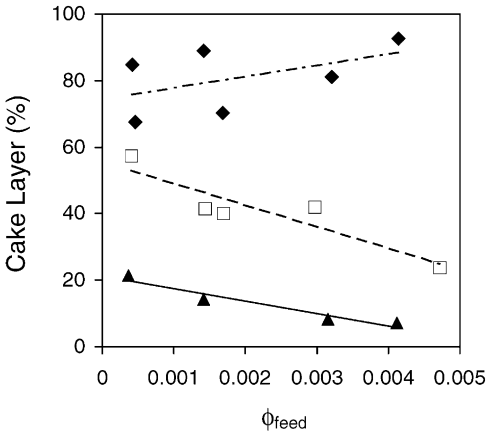

Fig. 6. Dependence of the percentage of particles in the cake layer on the inlet suspension concentration: (◆) 100 rpm ($Ta/Ta_c = 2.76$), (□) 200 rpm ($Ta/Ta_c = 5.51$), (▲) 400 rpm ($Ta/Ta_c = 11.02$). Lines are least squares fits to the data ($D_p = 22\,\mu m$, $D_{pore} = 10\,\mu m$, $Q_{in} = 6$ ml/s, 93% flow through filter).

At the highest rotational speed shown in Fig. 5 there is also little effect of feed rate.

Another important factor to consider is the effect of inlet concentration on the build-up of particles on the filter surface. To quantify the effect of inlet concentration, 15 trials were conducted varying the volume fraction ϕ_{feed} from approximately 0.00032–0.0047. Overall, the cake percentage does not depend strongly on the concentration of the inlet suspension, as shown in Fig. 6. Thus, rotating filtration's effectiveness is not limited to a narrow range of concentrations. In addition, further demonstrating the effectiveness of rotation, the results show that for higher rotational speeds the fraction of particles ending up in the cake layer decreases slightly with increasing particle concentration. To clarify, the actual number of particles in the cake layer actually increases with increasing concentration for the two higher rotational speeds, but a smaller fraction of particles entering the device end up in the cake layer. The result is similar to those seen previously [8], where higher feed concentrations resulted in lower filtrate fluxes at a given rotational speed. The postulate was that the decreasing fluxes were a result of increasing cake thickness with inlet feed concentration, consistent with the absolute increase in particles in the cake layer found here.

We also note here the scatter in the data indicated in Fig. 6. At the lowest concentration ($\phi_{feed} = 0.00032$) at 100 rpm, there is a significant difference in the measured cake layer for duplicate experiments. Furthermore, the scatter about the least squares fit through the data is substantially larger for the 100 rpm data than for the 400 rpm data where the cake layer is much smaller. This trend of greater scatter for larger cake layer percentages (above 70%) and less scatter for small and moderate cake layers is consistent throughout the data. It is probably a consequence of the difficulty in washing the cake layer off of the inner cylinder at the end of an experiment and collecting a suitable sample of the back-flush suspension, exacerbated for high particle counts in situations with substantial cake layers.

One of the key geometric parameters in rotating filtration is the combined effect of filter pore size and particle diameter, which can be examined using the ratio of particle size to pore size, D_p/D_{pore}. This ratio suggests the type of fouling that may occur [12]. Particles much larger than the pores ($D_p/D_{pore} > 1$) cause cake formation by collecting on the filter surface, sometimes directly blocking a pore. Particles near the filter pore size cause either pore blinding ($D_p/D_{pore} = 1$) or pore constriction ($D_p/D_{pore} < 1$). To test the effect of pore size and particle diameter, both were changed. A number of different polydisperse particles of varying sizes and densities (summarized in Table 2) were used with porous polyethylene filters having pore sizes of 5, 10, 15, and 60 μm. The results of changing the ratio of particle diameter to pore diameter are shown in Fig. 7. The advantage of faster rotation is evident at all particle sizes. The decrease in cake layer build-up with increasing ratio of particle diameter to pore diameter indicates that rotating filtration is especially effective against cake formation for larger particles. Previous experiments using suspensions of particles

Table 2
Properties of particles

Manufacturer	Material	Volumetric median diameter (μm)	Density (g/cm^3)
Potters Industries	Hollow glass spheres	14	1.12
Goodfellow Inc.	Nylon 6	22	1.16
CreaNova	Nylon	36	1.03
CreaNova	Nylon	62	1.03

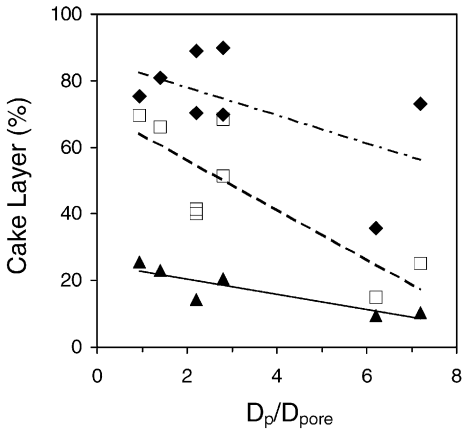

Fig. 7. Dependence of the percentage of particles in the cake layer on the ratio of particle diameter to filter pore diameter: (◆) 100 rpm ($Ta/Ta_c = 2.76$), (□) 200 rpm ($Ta/Ta_c = 5.51$), (▲) 400 rpm ($Ta/Ta_c = 11.02$). Lines are least squares fits to the data ($\phi_{feed} = 0.15\%$, $Q_{in} = 6$ ml/s, 93% flow through filter).

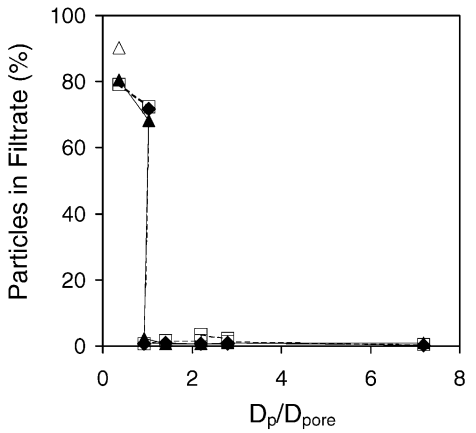

Fig. 8. Percentage of particles in the filtrate as a function of the ratio of particle diameter to pore diameter: (△) 50 rpm ($Ta/Ta_c = 1.38$), (◆) 100 rpm ($Ta/Ta_c = 2.76$), (□) 200 rpm ($Ta/Ta_c = 5.51$), (▲) 400 rpm ($Ta/Ta_c = 11.02$) ($\phi_{feed} = 0.15\%$, $Q_{in} = 6$ ml/s, 93% flow through filter).

with diameters of 26 and 12 μm showed a similar trend of decreasing fouling for increasing particle size [9]. However, their smallest particles with a diameter of 2 μm showed fouling levels between the other particle sizes, possibly caused by electrochemical interaction between the small particles and the filter material.

Previous research has suggested that particles in Taylor vortex flow that are denser than the fluid tend to end up on a single orbit around the vortex center (called a limit cycle orbit), irrespective of whether they start at the vortex center or near the cylinder walls [13]. An implication of this idea is that the centrifugal sedimentation, vortical motion, and shear related to the fluid flow field are adequate by themselves to prevent particles from even getting near the filter surface, regardless of the filter pore size. The hypothesis is that the hydrodynamic forces keep particles away from the membrane so that the physical barrier of pores smaller than the particles may not be necessary. To test this hypothesis, trials were done using particles smaller than the pore size in order to challenge the filter. The results in Fig. 8 show the percentage of inlet particles passing through the filter with the filtrate as a function of D_p/D_{pore}. A high percentage means very few particles were rejected. Even at high rotation speeds, the pores of the filter must be smaller than the diameter of the particles. The number of particles in the filtrate jumps to an unacceptable value when the ratio of the particle diameter to the pore diameter is less than one. Thus, a physical barrier to the particles is still necessary even though hydrodynamic forces reduce the tendency of particles to move toward the filter surface.

The effect of centrifugal sedimentation on preventing particles building up on the filter surface can be examined by calculating the effective terminal velocity of a particle in the rotating filter using a simplified analysis. In a rotating fluid field, a particle is subject to two radial forces. The centrifugal force due to the density difference between the particle and the fluid is directed radially outward for a particle denser than the fluid. The Stokes drag toward the filter surface is caused by the difference between the particle velocity, V_p, as it moves radially outward due to sedimentation and the fluid velocity, V_r, moving inward toward and through the filter (for the small particles in question, the Reynolds number based on the particle diameter and filtrate velocity is always less than 0.02, confirming the validity of the Stokes drag assumption). When these two forces balance, the particle is at its terminal velocity. The balance of the two forces is given by

$$(\rho_p - \rho_f)\frac{4}{3}\pi\left(\frac{D_p}{2}\right)^3 \Omega^2 r = 3\pi D_p \mu (V_p(r) - V_r(r)) \quad (1)$$

where ρ_f is the fluid density, and ρ_p the particle density. Both sides of the equation depend on the radial

position (r) of the particle. Since particles near the surface of the filter are the most critical, the inner radius r_i is used to calculate terminal velocity. Solving Eq. (1) for V_p at r_i yields

$$V_p(r_i) = \left[(\rho_p - \rho_f) \frac{D_p^2 \Omega}{18\mu} \right] r_i \Omega + V_r(r_i) \quad (2)$$

Note that the bracketed term on the right hand side of Eq. (2) is the particle Taylor number. While this crude estimate of the force balance on a particle neglects interactions with other particles and secondary flows, the direction and magnitude of the particles' terminal velocity calculated from Eq. (2) are indicative of the effectiveness of centrifugal sedimentation's contribution to minimizing the cake layer build-up. A negative terminal particle velocity indicates particle motion toward the filter surface and, thus, a tendency to increase cake layer build-up. A positive terminal velocity suggests that the centrifugal sedimentation is strong enough to carry the particle away from the filter surface, preventing cake layer build-up.

The cake layer percentage is plotted as a function of the terminal velocity for 44 experimental trials including a wide range of particle sizes and other experimental parameters in Fig. 9. Most trials have a negative terminal velocity, indicating that particles tend to move toward the rotating filter. The larger negative terminal velocities result in greater cake layers suggesting that the centrifugal effect plays a role

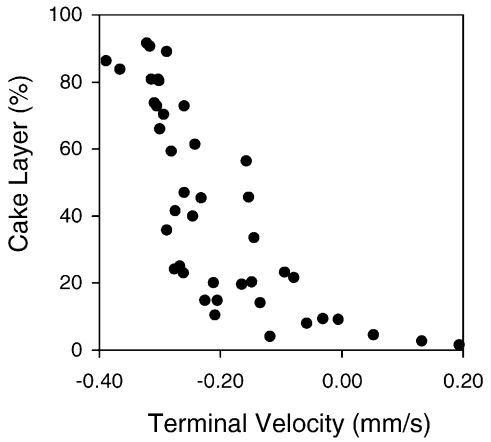

Fig. 9. Dependence of the percentage of particles in the cake layer on the terminal velocity of the particles ($D_{pore} = 10\,\mu m$, $Q_{in} = 6$ ml/s, $\phi_{feed} = 0.15\%$, 93% flow through filter).

in preventing cake layer build-up. However, the cake layer can be very small even though the terminal velocity is slightly negative. This discounts the centrifugal force as the major cake minimizing mechanism effect for this range of conditions. This also confirms reasoning behind the analysis of Beaudoin and Jaffrin [14], who used the balance of forces in Eq. (1) along with Darcy's law to define a critical pressure at which blood cells begin to deposit on a rotating filter blood plasma separator. They showed that the force balance between the drag force and the centrifugal force could not explain the improved flux for a rotating filter. Nevertheless, Fig. 9 suggests that the centrifugal effect is still important. There is a clear trend that shows as terminal velocity increases, cake layer decreases. For suspensions where the average particle has a positive terminal velocity, and, thus, tends to move away from the filter surface, there is almost no cake layer. As a point of reference, the radial fluid velocity (the second term on the right hand side of Eq. (2)) ranges from the same order of magnitude to two orders of magnitude larger than the centrifugal sedimentation velocity (the first term on the right hand side of Eq. (2)) and is of opposite sign (since $\rho_p > \rho_f$ and V_r is radially inward). Thus, under most filtration conditions, centrifugal sedimentation contributes to the reduction of particles getting near the filter surface in rotating filtration but is not enough by itself to prevent cake layer build-up.

Another primary geometric parameter of a rotating filter is the width of the gap between the rotating porous cylinder and the outer stationary cylinder. The effect of this gap on preventing particle build-up on the filter surface was investigated by changing the radius of the inner cylinder. The gap widths tested were $d = 0.17$, 0.30, and 0.72 cm corresponding to $d/D_p = 78$, 136, and 327. Changing the gap width also alters the aspect ratio so that $\Gamma = h/d = 75$, 42, and 18 and the radius ratio so that $\eta = r_i/r_o = 0.935$, 0.887, and 0.729 (the different radius ratios result in different critical Taylor numbers [11]). Fig. 10 shows the dependence of the percentage of particles in the cake layer on the annular gap. At the lowest rotational speed, changing gap width does not alter the cake layer. At higher rotational speeds, narrower gap widths reduce the cake layer. Even at the highest rotational speed, this dependence is quite evident, in contrast to some of the other filtration parameters studied. Vigo et al. [2], and Vigo and Uliana [7] found that decreasing the

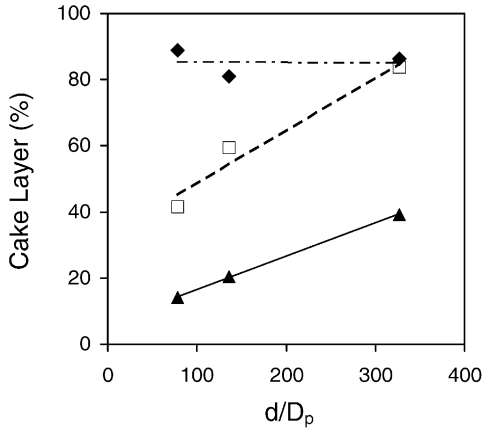

Fig. 10. Dependence of the percentage of particles in the cake layer on the annular gap width: (◆) 100 rpm ($2.76 \leq Ta/Ta_c \leq 17.52$), (□) 200 rpm ($5.51 \leq Ta/Ta_c \leq 35.05$), (▲) 400 rpm ($11.02 \leq Ta/Ta_c \leq 70.09$). Lines are least squares fits to the data ($D_p = 22\,\mu m$, $D_{pore} = 10\,\mu m$, $Q_{in} = 6$ ml/s, $\phi_{feed} = 0.15\%$, 93% flow through filter).

gap width increases filtrate flux, consistent with the reduced cake layer for decreasing gap widths that we found. At the lowest rotational speed that they considered, they found little effect due to gap width, similar to the 100 rpm results in Fig. 10. The increase in the cake layer with increasing gap width at higher speeds is clearly a consequence of the monotonic decrease in shear as the gap width increases. Thus, reducing the gap width is one of the critical parameters to reduce particles from plugging filter pores and cake layer build-up.

To this point, it is clear that increased shear in the annular gap minimizes the cake layer build-up in rotating filtration (Fig. 10). Centrifugal sedimentation aids in preventing cake layer build-up, but has a lesser role (Fig. 9). The vortical motion does not appear to play a direct role in preventing cake layer build-up (Fig. 4). The question that remains is whether it is the increased rotational shear or the increased axial shear that is key to reducing cake layer build-up. Both increase with decreasing gap width, so Fig. 10 does not help in determining which is more important. However, Fig. 4 indicates that rotational shear is more important for minimizing cake build-up than axial shear. In this figure, the axial shear is constant, but the increasing rotational shear causes reduced cake layer build-up. Nevertheless, two points must be made with regard to this conclusion. First, the axial shear can be the same order of magnitude as the rotational shear (although it is typically less). Thus, axial shear can sometimes play a role in preventing cake layer build-up. Second, although the vortices themselves do not appear to reduce cake layer build-up, the vortical motion redistributes the angular momentum resulting in steeper azimuthal velocity gradients and higher shear at the inner cylinder [15,16]. Thus, the vortical motion reduces cake layer build-up indirectly by increasing the rotational shear. In summary, rotational shear, which can be controlled independent of the suspension flow rate, seems to be key to preventing cake layer build-up in a rotating filter. However, the rotational shear is increased as a result of the vortical motion and is enhanced by the axial shear related to the suspension flow rate, while centrifugal sedimentation slows particle motion toward the filter surface, all aiding in minimizing cake layer build-up.

4. A fundamental governing parameter

Because of the large number of experimental variables in rotating filtration, it is desirable to identify a single scaling parameter that could govern the design of rotating filters for a wide range of conditions. Other researchers studying rotating filtration and cross-flow filtration have attempted to identify a parameter that predicts the prevention of particles building up on the filter surface. For instance, Beaudoin and Jaffrin [14] suggested using the shear rate at the filter surface. For the thin gap of a rotating filter, the rotational shear rate can be approximated as

$$\gamma_w = \frac{\Omega r_i}{d} \tag{3}$$

The velocity across the gap is not linear as suggested by Eq. (3) because the vortices redistribute the azimuthal momentum, resulting in a nearly uniform azimuthal velocity profile in the center of the gap with high velocity gradients near the walls of the annulus [15,17]. However, a linear profile provides a reasonable order of magnitude estimate of the shear rate.

The percentage of particles ending up in the cake layer as a function of the shear rate is shown in Fig. 11a for 77 trials changing the rotation rate, the filtrate flow as a percentage of inlet flow, the total suspension flow,

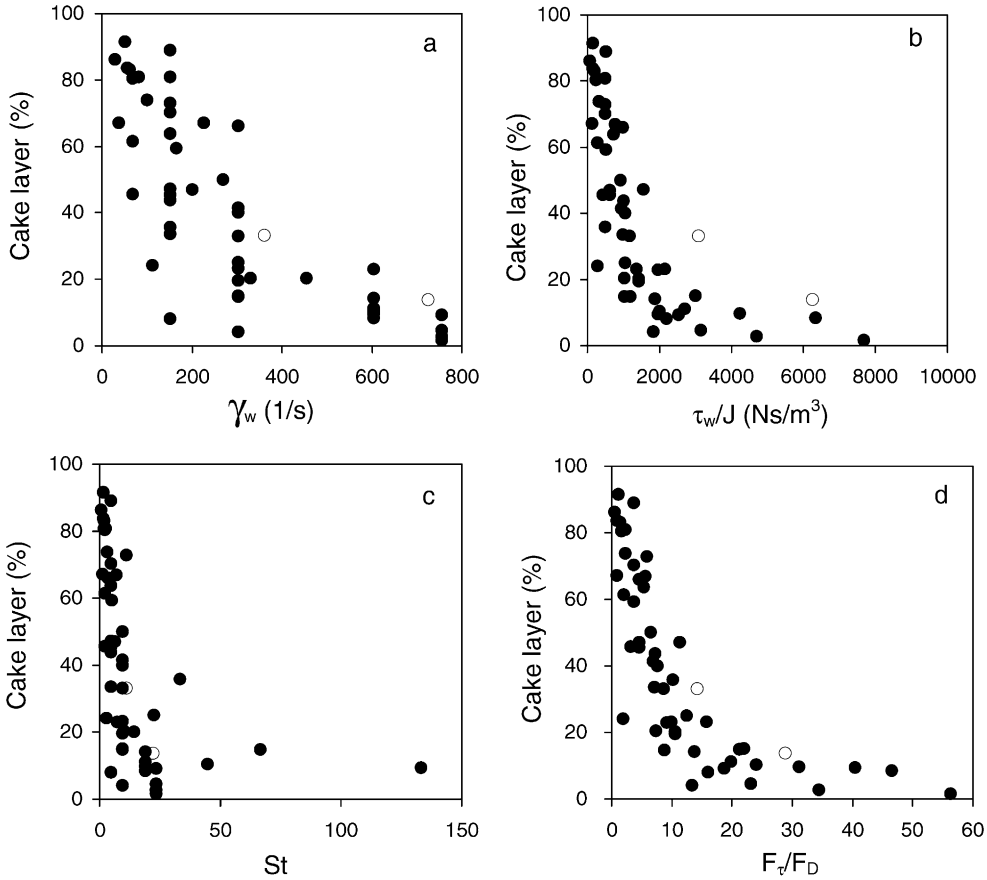

Fig. 11. Comparison of scaling parameters for rotating filtration.

the particle size, the fluid viscosity, the fluid density, the particle density, the concentration, the filter pore size, and the gap width. A rough correlation between cake layer and shear rate indicates that the rotational shear rate is an important factor in the tendency for rotation filtration to prevent the build-up of particles on the filter surface. However, the wide spread in the data would make it difficult to optimize a device for a given set of filtration conditions based on the shear rate.

More recently, the ratio of flux through the filter (J) to the shear stress at the wall τ_w has been proposed as the critical parameter that characterizes the anti-fouling character [18,19]. This ratio represents the mass transport toward the membrane by convection divided by the mass transfer away from it by erosion and shear-induced migration. The data from the same 77 trials are plotted as a function of this ratio in Fig. 11b. The collapse of the data is much better than in Fig. 11a, since this ratio accounts for the force driving particles toward the filter as well as that keeping particles away from the filter. However, there is still some spread in the data. An additional flaw in using this ratio can be seen when considering variation in viscosity. The two data points represented with open symbols in Fig. 11b are for experimental trials using a mixture of glycerin and water, instead of pure water, resulting in a viscosity 2.41 times that of water. The high viscosity of this mixture causes high shear stress, and thus, high values of τ_w/J. However, this higher shear stress does not result in lower cake layer values.

In addition to problems with data collapse, the two previous parameters are dimensional. A parameter

that provides a non-dimensional scaling is the particle Stokes number, which represents the ability of the particles to follow the motion of the carrier fluid. In the geometry of the rotating filter the particle Stokes number is expressed as

$$St = \frac{1}{18}\rho_p \frac{D_p^2 \Omega r_i}{\mu d} \tag{4}$$

The dependence of the percentage of particles remaining in the cake layer on the Stokes number is shown in Fig. 11c. While the collapse of the data is reasonable, there are several problems with this parameter. First, the trials with the highest Stokes numbers are not the trials with the least cake layer. Second, several trials have identical Stokes numbers and widely differing cake layers. For example, for a Stokes number of 4.7, the cake percentage varies from 8 to 89%. The problem with using the Stokes number to predict the tendency to prevent particles building up on the filter surface lies with the absence of a measure of the force driving the particles toward the filter surface. Thus, trials that differ only in the filtrate flow rate will have identical Stokes numbers but widely varying cake layer percentages.

The most influential forces acting on a particle near the filter surface can be used to develop the ideal fundamental parameter. The force that induces the mass transport of particles toward the filter surface is the Stokes drag due to the filtrate flux. The results from Section 3 indicate that rotational shear dominates over the centrifugal force and vortical motion in acting against the filtrate flux moving the particles toward the filter surface. Thus, the Stokes drag toward the filter is counteracted by erosion and shear-induced migration of particles from the filter surface caused by the shear stress. The associated force is the shear stress multiplied by the particle surface area. This force acts parallel to the filter surface and perpendicular to the Stokes drag. The ratio between the shear force and the Stokes drag for the geometry of a rotating filter can be written as

$$\frac{F_\tau}{F_D} = \frac{\text{Shear force}}{\text{Stokes drag}} = \frac{\mu \Omega r_i \pi D_p^2/d}{3\pi \mu D_p V_r} \tag{5}$$

which can be simplified to

$$\frac{F_\tau}{F_D} = \frac{1}{3}\left(\frac{V_\theta}{V_r}\right)\left(\frac{D_p}{d}\right) \tag{6}$$

where $V_\theta = \Omega r_i$ is the tangential velocity based on the speed of the inner cylinder, V_r the radial velocity based on the overall filtrate flow rate, D_p the particle diameter, and d is the gap between the two cylinders. This ratio is intuitively pleasing for a number of reasons. First, it is non-dimensional and, thus, can be used to scale a wide variety of filtration systems. Second, it takes into account the variables that have been shown to have a large effect on the cake layer build-up in rotating filtration including the filtrate flux, the rotational speed, the particle diameter, and the gap width.

The data for the 77 experimental trials are plotted against this ratio in Fig. 11d. Clearly, there is a strong dependence of the percentage of particles remaining in the cake layer on this ratio with the data collapsing substantially better than for the other scaling parameters. When the ratio exceeds 20, the build-up of the cake layer is minimal. Below this number, the cake layer is substantial. This collapse of the data further confirms that the primary mechanism in rotating filtration that reduces cake layer build-up is the shear due to rotation. The fact that the data does not collapse completely shows that rotational shear is not the only mechanism affecting the build-up of particles near the filter surface for rotating filtration. Centrifugal sedimentation and axial shear, though of lesser importance, also play a role. In addition, this simple estimate of the shear used in Eq. (5) does not reflect the details of the complicated vortical flow field related to the Taylor vortices that increase the shear at the surface of the filter.

5. Conclusions

The results of this study provide the following guidelines to optimize the design of a rotating filter. For a given filtration problem with the type of the suspension and the desired filtrate flow rate specified, the following design guidelines can be used.

- The filter pores should be smaller the particle diameter.
- The gap width between the inner and outer cylinder should be as small as possible, with allowances made for manufacturing tolerances and particle size.
- The rotational speed should be higher for smaller particles than that for larger particles.

- If high concentration ratios are needed, the rotational speed should be higher.
- High concentration suspensions are more effectively separated than low concentration suspensions, based on the cake percentage, although the actual number of particles building up on the surface may be quite large.
- The shear force on a particle should be at least an order of magnitude larger than the Stokes drag to minimize cake layer formation.

Cross-flow filtration and rotating filtration are somewhat similar in that there is relative tangential motion between the filter surface and the suspension. Thus, the last guideline may also be helpful in designing cross-flow filters.

While this study focused on the build-up of a cake layer on the filter surface, it is reasonable to expect that the design recommendations presented here should also be applicable to minimizing the plugging of membrane pores by particles and to reducing the concentration polarization in rotating cylindrical filters.

Acknowledgements

This work was supported by NASA (NASA Grant NAG9-1053). The authors thank Ms. Karen Pickering for her support and advice regarding the filtration experiments.

References

[1] D. Hallström, M. Lopez-Leiva, Description of a rotating ultrafiltration module, Desalination 24 (1978) 273–279.
[2] F. Vigo, C. Uliana, P. Lupino, The performance of a rotating module in oily emulsions ultrafiltration, Sep. Sci. Technol. 20 (1985) 213–230.
[3] K. Ohashi, K. Tashiro, F. Kushiya, T. Matsumoto, S. Yoshida, M. Endo, T. Horio, K. Ozawa, K. Sakai, Rotation-induced Taylor vortex enhances filtrate flux in plasma separation, Trans. Am. Soc. Artif. Intern. Organs 34 (1988) 300–307.
[4] A. Rushton, G.S. Zhang, Rotary microporous filtration, Desalination 70 (1988) 379–394.
[5] K.H. Kroner, V. Nissinen, Dynamic filtration of microbial suspensions using an axially rotating filter, J. Membr. Sci. 36 (1988) 85–100.
[6] P. Mikulasek, P. Dolecek, Use of a rotating filter to enhance ceramic membrane filtration performance of latex dispersions, Sep. Sci. Technol. 29 (1994) 1943–1956.
[7] F. Vigo, C. Uliana, Influence of the vorticity at the membrane surface on the performances of the ultrafiltration rotating module, Sep. Sci. Technol. 21 (1986) 367–381.
[8] J.Y. Park, C.K. Choi, J.J. Kim, A study on dynamic separation of silica slurry using a rotating membrane filter, J. Membr. Sci. 97 (1994) 263–273.
[9] G. Belfort, P. Mikulasek, J. Pimbley, K.Y. Chung, Diagnosis of membrane fouling using a rotating annular filter 2: dilute particle suspensions of known particle size, J. Membr. Sci. 77 (1993) 23–39.
[10] G.I. Taylor, Stability of a viscous liquid contained between two rotating cylinders, Philos. Trans. A 223 (1923) 289–343.
[11] A. Recktenwald, M. Lucke, H.W. Muller, Taylor vortex formation in axial through flow: linear and weakly non-linear analysis, Phys. Rev. E 48 (1993) 4444–4454.
[12] M. Elimelech, J. Gregory, X. Jia, R.A. Williams, Particle Deposition and Aggregation, Butterworths, London, 1995.
[13] S.T. Wereley, R.M. Lueptow, Inertial particle motion in a Taylor–Couette rotating filter, Phys. Fluids 11 (1999) 325–333.
[14] G. Beaudoin, M.Y. Jaffrin, Plasma filtration in Couette flow membrane devices, Artif. Organs 13 (1989) 43–51.
[15] S. Wereley, R.M. Lueptow, Azimuthal velocity in supercritical circular Couette flow, Exp. Fluids 18 (1994) 1–9.
[16] A. Akonur, R. M. Lueptow, Three-dimensional velocity field for non-wavy and wavy Taylor–Couette flow, J. Fluid Mech. (2002), in review.
[17] P. Marcus, Simulation of Taylor–Couette flow. Part 2. Numerical results for wavy-vortex flow with one traveling wave, J. Fluid Mech. 146 (1984) 65–111.
[18] M.C. Aubert, M.P. Elluard, H. Barnier, Shear stress induced erosion of filtration cake studied by a flat rotating disk method: determination of the critical shear stress of erosion, J. Membr. Sci. 84 (1993) 229–240.
[19] G. Gesan, G. Daufin, U. Merin, Performance of whey cross-flow microfiltration during transient and stationary operating conditions, J. Membr. Sci. 104 (1995) 271–281.